



RESEARCH ARTICLE

10.1029/2021EF002537

†These authors contributed equally to the work described in this manuscript.

Key Points:

- Climate change enhanced the precipitation associated with the February 2017 atmospheric river over Northern California
- The two distinct pulses comprising this event were differentially impacted
- A stronger thermodynamic response during the second pulse enabled a precipitation increase more than double that of the first pulse

Supporting Information:

Supporting Information may be found in the online version of this article.

Correspondence to:

A. C. Michaelis,
amichaelis@niu.edu

Citation:

Michaelis, A. C., Gershunov, A., Weyant, A., Fish, M. A., Shulgina, T., & Ralph, F. M. (2022). Atmospheric river precipitation enhanced by climate change: A case study of the storm that contributed to California's Oroville Dam crisis. *Earth's Future*, 10, e2021EF002537. <https://doi.org/10.1029/2021EF002537>

Received 5 NOV 2021

Accepted 31 JAN 2022

Author Contributions:

Conceptualization: Allison C. Michaelis, Alexander Gershunov, Alexander Weyant, Meredith A. Fish, F. Martin Ralph

Formal analysis: Allison C. Michaelis, Alexander Weyant, Tamara Shulgina

Funding acquisition: F. Martin Ralph

Investigation: Allison C. Michaelis

Methodology: Allison C. Michaelis

Visualization: Alexander Weyant, Tamara Shulgina

© 2022 The Authors. Earth's Future published by Wiley Periodicals LLC on behalf of American Geophysical Union. This is an open access article under the terms of the [Creative Commons Attribution License](https://creativecommons.org/licenses/by/4.0/), which permits use, distribution and reproduction in any medium, provided the original work is properly cited.

Atmospheric River Precipitation Enhanced by Climate Change: A Case Study of the Storm That Contributed to California's Oroville Dam Crisis

Allison C. Michaelis¹† , Alexander Gershunov²† , Alexander Weyant²†, Meredith A. Fish^{3,4}, Tamara Shulgina², and F. Martin Ralph²

¹Department of Earth, Atmosphere, and Environment, Northern Illinois University, DeKalb, IL, USA, ²Center for Western Weather and Water Extremes, Scripps Institution of Oceanography, University of California San Diego, La Jolla, CA, USA, ³Department of Earth and Planetary Sciences, Rutgers Institute of Earth, Ocean, and Atmospheric Sciences, Rutgers University, New Brunswick, NJ, USA, ⁴Rutgers Institute of Earth, Ocean, and Atmospheric Sciences, Rutgers University, New Brunswick, NJ, USA

Abstract An increasingly volatile hydroclimate increases California's reliance on precipitation from atmospheric rivers (ARs) for water resources. Here, we simulate the AR that contributed to the Oroville Dam crisis in early February 2017 under global climate conditions representing preindustrial, present-day, mid-, and late-21st century environments. This event consisted of two distinct AR pulses: the first snowy, westerly, and cool followed by a southwesterly and warm pulse resulting in copious rain-on-snow. We estimate that climate change to date results in ~11% and ~15% increase in precipitation over the Feather River Basin in Northern California for the first and second pulses, respectively, with late-21st century enhancements upwards of ~21% and ~59%, respectively. Although both pulses were enhanced by the imposed climate changes, the thermodynamic response and subsequent precipitation increases were most substantial during the second pulse. The disparate changes demonstrated here highlight that not all ARs will respond similarly in a warmer world.

Plain Language Summary California's reliance on precipitation from atmospheric rivers is expected to increase as our climate warms. Understanding how climate change is impacting this increasingly dominant mode of precipitation is vitally important for water-resource management throughout the state, across the North American West Coast, and for other similarly impacted regions. Our case study of an impactful atmospheric river from early February 2017 that contributed to the Oroville Dam crisis in Northern California, modeled under preindustrial, present-day, mid-, and late-21st century unabatedly warming environments, demonstrates an overwhelming increase in precipitation throughout the event. This particular storm was comprised of two distinct pulses, and while both pulses of the storm are enhanced in the warmer future epochs, the estimated precipitation increases are disproportionately higher for the second pulse due to larger increases in temperature and moisture. Our results therefore suggest that not all atmospheric rivers are similarly affected by climate change and point to specific directions for relevant future research.

1. Introduction

California's hydroclimate is dominated by extreme precipitation associated with atmospheric rivers (ARs), resulting in impressive volatility of the region's Mediterranean precipitation regime marked by wild swings between deficient and excessive water years where the relative presence (or absence) of intense ARs is associated with historic challenges in water resource management (Dettinger et al., 2011; Gershunov et al., 2017; Guan et al., 2010; Swain et al., 2018). Climate change is contributing, and is expected to contribute further, to existing water-resource challenges in the region by eroding mountain snowpack (Knowles et al., 2006; Mote et al., 2019; Rhoades et al., 2018) and reducing the frequency of precipitation (Johanson & Fu, 2009; Luković et al., 2021; Pierce et al., 2013; Polade et al., 2014, 2017). Extreme precipitation events in California, however, are projected to become stronger and more frequent, mainly due to more potent (i.e., wetter, wider, and longer) ARs in a warmer climate (Baek & Lora, 2021; Gershunov et al., 2019; Huang et al., 2020; Polade et al., 2017). This combination of less frequent but more intense precipitation boosts the natural variability of the annual hydroclimate by increasing the risk of drought and enhancing California's reliance on extreme ARs for the generation of water

Writing – original draft: Allison C. Michaelis, Alexander Gershunov, Tamara Shulgina

Writing – review & editing: Alexander Weyant, Meredith A. Fish, F. Martin Ralph

resources, thus exacerbating challenges in water resource management in a future, warmer world (Gershunov et al., 2019; Rhoades et al., 2020).

Such projected changes to California's hydroclimate come with heightened risks of flooding and infrastructure damage, especially given the region's aging engineered water management systems. A recent crisis of this nature was nearly averted at Oroville Dam on the Feather River in Northern California in early February 2017 during a historically active season for ARs in California (Gershunov et al., 2017; Moore et al., 2020; White et al., 2019). An AR family (Fish et al., 2019) in early February 2017 featuring two successive pulses of enhanced vertically integrated horizontal vapor transport (IVT) led to prolonged AR conditions, excessive precipitation, and rain-on-snow over the already saturated Feather River Basin (FRB; Henn et al., 2020; White et al., 2019). Excessive runoff subsequently contributed to conditions that damaged the Oroville Dam's main and emergency spillways, leading to acute concerns of catastrophic structural failure and prompting evacuation of 188,000 people; subsequent repairs totaled ~\$1 billion (Henn et al., 2020; Vano et al., 2018; White et al., 2019). This incident highlights the hazards involved in mitigating flood risks while simultaneously trying to derive water resources from floodwater—a situation California will increasingly need to manage heading into a warmer, more volatile future (Gershunov et al., 2019; Polade et al., 2017).

Global climate models (GCMs) project an increasing trend in AR activity, particularly landfalling ARs along the California Coast (Gershunov et al., 2019; Payne et al., 2020; Rhoades et al., 2020; Zhang et al., 2021), as well as increased occurrence, intensity, and duration of drought (Cayan et al., 2010; Luković et al., 2021; Williams et al., 2020), thus enhancing the volatility of California's water resources (Gershunov et al., 2019; Polade et al., 2014, 2017; Swain et al., 2018). Event-scale analyses of ARs in a projected future climate-change framework (e.g., Huang et al., 2020; Mahoney et al., 2018; Singh et al., 2018) remain limited, particularly high-resolution case studies (Kossin et al., 2017; Payne et al., 2020). Given that ARs move near-saturated air (Cobb et al., 2021; Neiman et al., 2013; Ralph et al., 2005) and generate largely orographic precipitation (Neiman et al., 2008; Ralph et al., 2005), we expect a relatively clear relationship between a warming climate, AR intensity, and resultant precipitation to emerge (Baek & Lora, 2021; Gao et al., 2015; Gershunov et al., 2019; Huang et al., 2020; Lavers et al., 2015; Ma et al., 2020; Payne et al., 2020; Rhoades et al., 2020; Warner et al., 2015; Zhang et al., 2021). Here, we explore this expected connection with respect to precipitation, explicitly focusing on the AR family contributing to the February 2017 Oroville Dam crisis: hereafter referred to as the Oroville AR, AR event, or “the AR”.

2. Model Simulations

We simulated the Oroville AR using version 7.0 of the Model for Prediction Across Scales-Atmosphere (MPAS-A; Skamarock et al., 2012). MPAS-A is a global, atmosphere-only, nonhydrostatic numerical model utilizing variable-resolution horizontal grids created with unstructured Voroni meshes (Du et al., 1999), allowing for the gradual coarsening from localized areas of high resolution within a single domain, thus alleviating any discontinuities typical of traditional nesting approaches (Park et al., 2014). Here, we used the 3–60 km variable resolution mesh with the 3-km area centered on 37°N, 126°W to encompass the entirety of the state of California and ~15° offshore into the Pacific Ocean (not shown).

Following a method similar to Michaelis et al. (2019), we performed dynamical ensemble simulations akin to pseudo-global warming (PGW) experiments (e.g., Hara et al., 2008; Lackmann, 2013; Mallard et al., 2013; Rasmussen et al., 2011; Schär et al., 1996), simulating the AR in past (representative of preindustrial 1,900), present (representative of present-day), near-future (representative of 2,050), and future (representative of 2,100) climate conditions by adding (or subtracting) monthly averaged temperature changes for February derived from a subset of 20 GCMs from the Coupled Model Intercomparison Project Phase 5 (CMIP5; see Michaelis et al., 2019, their Table 2) to the initial condition temperatures at all pressure levels, sea-surface, and deep-soil levels. The temperature changes, or “deltas”, for the past climate simulations were calculated by subtracting the 1880–1899 average February temperature from the 1980–1999 average February temperature. Similarly, the temperature deltas for the near-future and future climate simulations are calculated by subtracting the 1980–1999 average February temperature from the 2040–2059 and 2080–2099 average February temperatures, respectively, following the high-end Representative Concentration Pathways (RCP) 8.5 emissions scenario. The delta patterns for sea-surface temperatures over the eastern Pacific largely exhibit warming trends with increasing magnitudes

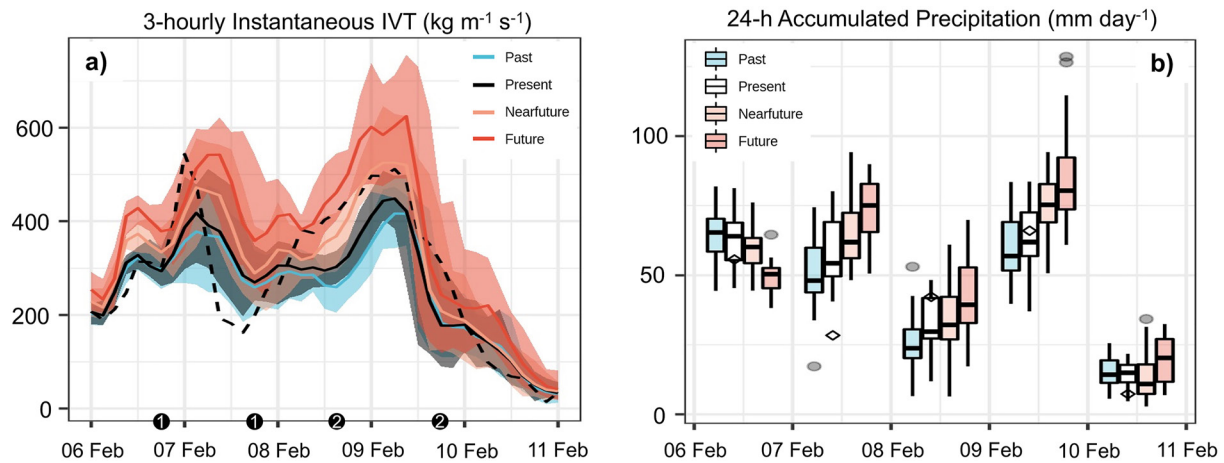


Figure 1. (a) Time series of 3-hourly instantaneous IVT ($\text{kg m}^{-1} \text{s}^{-1}$) averaged over the Feather River basin from 12 UTC 6 February to 12 UTC 11 February 2017 for the (dashed black) ERA5, (blue) past, (black) present, (orange) near-future, and (red) future epochs. Ensemble mean values are plotted in the solid lines with shading representing the ensemble spread. Start and end times for the two AR pulses are indicated with numbered circles on the x-axis. (b) Box-and-whisker plots of 24-hr accumulated precipitation (mm day^{-1}) for (diamonds) PRISM, (blue) past, (white) present, (orange) near-future, and (red) future epochs. The upper (lower) whiskers extend from the maximum (minimum) value to the 75th (25th) percentile. Outlying values (defined as 1.5 times the interquartile range) are shown in the gray circles.

from past to future; the largest increases occur poleward of 50°N , and the smallest changes are found in the midlatitudes between 30°N and 40°N (Figure S1 in the Supporting Information S1). Based on the imposed temperature changes, geopotential height and specific humidity are adjusted accordingly by the model. We hold relative humidity constant at the initial time; however, this constraint is not necessarily retained throughout the model simulations due to the lack of imposed boundary conditions. Carbon dioxide (CO_2) concentrations in the past, near-future, and future simulations are altered to 296, 541, and 936 ppm, respectively, following the RCP8.5 projections provided by Meinshausen et al., 2011; present-day CO_2 concentrations were used in the present-climate simulations. We replaced analyzed sea ice in the initial conditions with the respective 20-year GCM ensemble median sea ice for February in all simulations; sea ice extent and sea-surface temperatures do not vary over the six-day simulations. While the 1980–1999 CMIP5 GCM ensemble median sea ice does not exactly match the present-day analyzed sea ice extent (not shown), our method ensures that sea ice is handled consistently in all simulations. We chose to use the ensemble median sea ice over the ensemble mean to avoid an overly diffuse ice edge (Michaelis et al., 2019).

We created an ensemble of simulations in each climate regime by varying the MPAS-A initial conditions using the 21-member Global Ensemble Forecast System (GEFS) where each ensemble member is slightly perturbed from the original observations, resulting in a total of 84 simulations (21 for each climate scenario). All simulations employ the same model configuration with 55 vertical levels, a model top of 30 km, and the following physics parameterizations: the scale-aware Grell-Freitas convective parameterization scheme, non-aerosol aware Thompson microphysics parameterization scheme, the MYNN boundary layer and surface layer parameterization schemes, the Rapid Radiative Transfer Model (RRTMG) long- and short-wave radiation parameterization schemes, and the Noah land-surface model. These physics choices are recommended by MPAS-A as part of the “convection permitting” physics suite for use in any simulations employing meshes with horizontal grid spacing <10 km.

All simulations are initialized at 12 UTC 5 February 2017 and integrated through 12 UTC 11 February 2017; output is recorded every 3-hr and the first 24-hr are discarded as spin-up to the imposed changes described above. Our analysis period is therefore a 120-hr period from 12 UTC 6 February through 12 UTC 11 February. To determine the time windows of the two AR pulses associated with the Oroville AR as discussed in the following analysis, we first identified the times of maximum IVT based on the 3-hourly IVT time series from the MPAS-A present-day ensemble mean. We found these IVT peaks occur at 15 UTC 7 February for the first pulse and 18 UTC 9 February for the second pulse (Figure 1a). We then identified the local minima preceding and following each peak as the start and end times for the pulse windows, respectively. The time window for the first pulse is

therefore taken as the 24-hr period from 06 UTC 7 February to 06 UTC 8 February 2017. For the second pulse, the time window is defined as the 27-hr period from 03 UTC 9 February to 06 UTC 10 February.

3. Observed Event Characteristics and Present-Day Simulations

The Oroville AR occurred between 6 and 11 February 2017 as two successive midlatitude cyclones in the eastern North Pacific basin moved onshore, creating multiple pulses of elevated IVT, and leading to sustained AR conditions (i.e., $IVT \geq 250 \text{ kg m}^{-1} \text{ s}^{-1}$) over the FRB for several days (Moore et al., 2020; White et al., 2019). The two AR pulses were quite distinct, both in terms of IVT orientation and temperature. The first pulse on 7 February was westerly and cool, producing significant snow on top of an already impressive snowpack that had accumulated in the months leading up to the AR (Figure S2 in the Supporting Information S1; Henn et al., 2020; Moore et al., 2020; White et al., 2019). The second pulse on 9 February had a more southerly orientation, was warmer with a higher snowline, and produced comparable amounts of total precipitation with more rain and less snow (Figures S2 and S3 in the Supporting Information S1; Henn et al., 2020; Moore et al., 2020; White et al., 2019). Melting due to rain-on-snow produced extreme runoff with snowmelt contributing between 25% and 50% of the total runoff (Henn et al., 2020) and reservoir inflow from the AR (Figure S3 in the Supporting Information S1). Due to the nature of the Oroville AR and the deep antecedent snowpack, this event, particularly its second pulse, although not exceptional in and of itself, was an extreme and efficient runoff producer, thus multiplying the AR's impacts on Oroville Dam.

Compared to ground-truth, taken as the ERA5 reanalysis (Hersbach et al., 2020) for IVT and Parameter-elevation Regression on Independent Slopes Model (PRISM; Daly et al., 2008) for precipitation, the present-day MPAS-A simulations did quite well at representing the timing and magnitude of AR intensity (i.e., IVT) and precipitation over the FRB during the second AR pulse from 03 UTC 9 February through 06 UTC 10 February (Figure 1). During the first pulse, on the other hand, from 06 UTC 7 February through 06 UTC 8 February, the present-day ensemble mean precipitation was overestimated compared to observations (Figure 1b). While the present-day ensemble mean peak IVT over the FRB was underestimated by MPAS-A, the duration of the first pulse was longer (Figure 1a), likely contributing to an increase in precipitation relative to PRISM. The ERA5 IVT, however, was consistently within 19% of the present-day MPAS-A ensemble spread, indicating that MPAS-A performed reasonably well at representing the IVT magnitudes throughout the duration of the event. Discrepancies in simulated IVT and precipitation magnitude are likely due to slight errors in the simulated AR position as well as the coarser topography of ERA5 compared to MPAS-A.

During the 24-hr period surrounding the first AR pulse, $\sim 68 \text{ mm}$ of precipitation fell over the FRB in the present-day MPAS-A ensemble mean with an average IVT over the basin of $\sim 343 \text{ kg m}^{-1} \text{ s}^{-1}$ (maximum IVT of $\sim 472 \text{ kg m}^{-1} \text{ s}^{-1}$; Figure 1; Figure S4 in the Supporting Information S1). A total of $\sim 69 \text{ mm}$ of precipitation fell during the second AR pulse with an average IVT over the basin of $\sim 346 \text{ kg m}^{-1} \text{ s}^{-1}$ (maximum IVT of $\sim 476 \text{ kg m}^{-1} \text{ s}^{-1}$; Figure 1; Figure S4 in the in the Supporting Information S1). MPAS-A also reproduced the distinct nature of the two IVT pulses. The first pulse of the present-day simulated AR was westerly $\sim 254^\circ$ (Figure 2a) with a midlevel temperature over the FRB of $\sim 3^\circ\text{C}$ (Figure 3), while the second, southwesterly pulse $\sim 212^\circ$ (Figure 2b) was warmer with a mid-level temperature of $\sim 6^\circ\text{C}$ (Figure 3).

Despite slight discrepancies between the present-day MPAS-A ensemble mean and observations (i.e., ERA5 and PRISM), MPAS-A replicates the main behavior of the Oroville AR: two distinct pulses with different orientations and mid-level temperatures, but with roughly equal IVT and precipitation magnitudes over the FRB. As such, the present-day MPAS-A remains an adequate basis for assessing climate change contributions to precipitation related to the Oroville AR.

4. Climate Change Impacts

As is typical for ARs, which produce mainly orographic precipitation (Neiman et al., 2008; Ralph et al., 2005), the bulk of event total precipitation accumulating in the FRB fell on the west-southwest-facing slope of the Sierra Nevada above Lake Oroville during both AR pulses (Figures 2c–2e). Evolving global warming enhances precipitation from the AR (Figure 1b) in accordance with orography: a similar spatial pattern with further projected

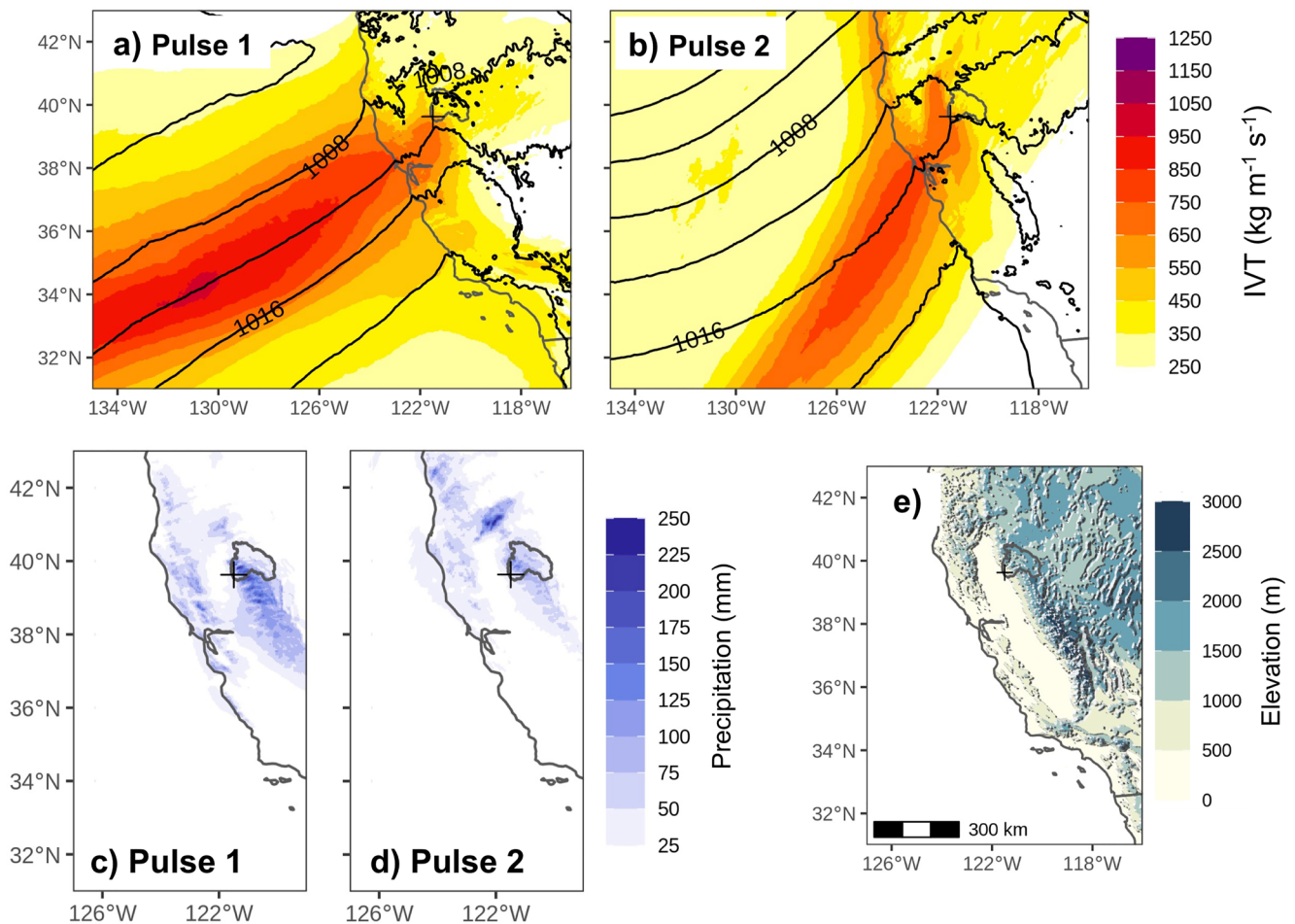


Figure 2. MPAS-A present-day ensemble mean IVT ($\text{kg m}^{-1} \text{s}^{-1}$; shading) and SLP (hPa; black contours) for (a) 15 UTC 7 February 2017 and (b) 18 UTC 9 February 2017 during the first and second AR pulses, respectively. MPAS-A present-day ensemble mean precipitation (mm) accumulated over the (c) first AR pulse from 06 UTC 7 February to 06 UTC 8 February and (d) second AR pulse from 03 UTC 9 February to 06 UTC 10 February. (e) Topography throughout the state of California as represented by MPAS-A. The Feather River Basin is outlined in gray, and the Oroville Dam location is indicated by a “+” in all panels.

warming indicates the largest precipitation increases on the windward slope of the Sierra Nevada, particularly the FRB, and primarily during the second pulse (Figure 4).

Our experiments indicate that climate change to date (i.e., comparing past to present-day) boosted precipitation from the AR during the first pulse by about 11% (~ 7 mm) on average over the FRB. Changes over the basin during the second pulse were larger with around a 15% (~ 9 mm) increase (Figures 4a and 4d). Considering the anomalously wet winter even prior to the AR (Gershunov et al., 2017; Moore et al., 2020; Vano et al., 2018; White et al., 2019), we hypothesize that runoff efficiency was high (Figure S3 in the Supporting Information S1) and that much of this enhanced rainfall flowed quickly into Lake Oroville (Henn et al., 2020). Moreover, given the extensive preexisting snowpack, snowmelt due to rain-on-snow contributed substantially to the runoff generated by the AR (\sim about 37%; Henn et al., 2020). The first pulse of the AR contributed over 100 thousand acre-feet (TAF) to the existing snowpack on 7 February, while the second, warmer pulse, effectively melted ~ 150 TAF between 9 and 10 February (Figure S2 in the Supporting Information S1), essentially negating the previous snowpack gains. The additional warmth of the AR due to global warming since 1900, no doubt contributed to the impressive ensuing runoff by elevating the snowline associated with the storm, particularly during its warmer final pulse (Figure 3). This spatial pattern of precipitation enhancement from past to present epochs (Figures 4a and 4d) is mainly due to the increased moisture content of the AR with warming (Figure 5) and the stationarity of the mountains on the relevant timescales involved in anthropogenic climate change.

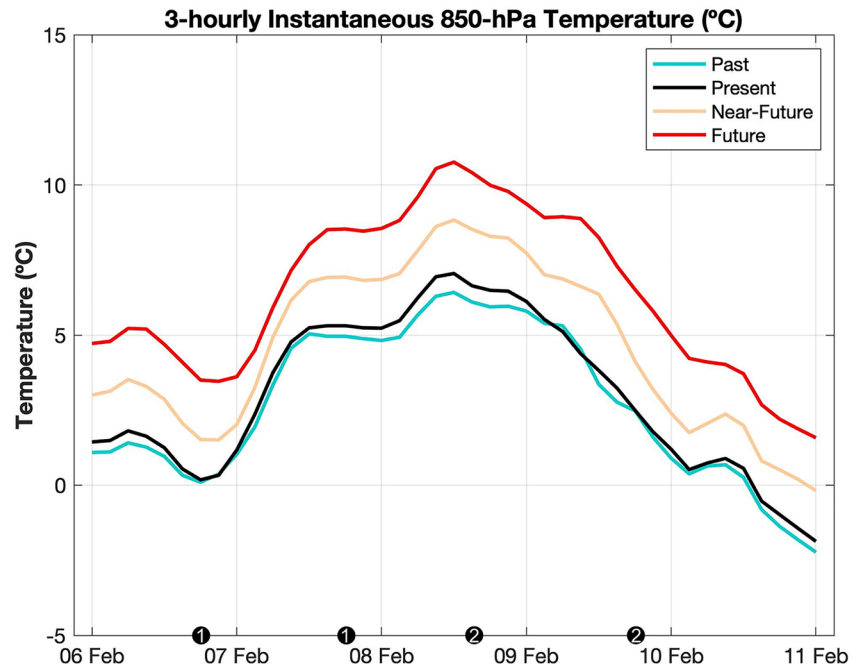


Figure 3. MPAS-A ensemble mean 850-hPa temperature ($^{\circ}\text{C}$) averaged over the Feather River Basin for the (blue) past, (black) present, (orange) near-future, and (red) future epochs every 3-hr from 12 UTC 6 February through 12 UTC 11 February 2017. Start and end times for the two AR pulses are indicated with numbered circles on the x -axis.

Interestingly, present-to-near-future and present-to-future changes in precipitation are not uniform over the two AR pulses. Average precipitation over the FRB during the first pulse increases by $\sim 9\%$ and $\sim 21\%$ in each epoch, respectively (Figures 4b and 4c). The precipitation enhancement during the second pulse is considerably greater with increases of $\sim 26\%$ and $\sim 59\%$, in near-future and future epochs, respectively (Figures 4e and 4f). Both pulses exhibit modest changes in landfalling orientation between present, near-future, and future climates (not shown), suggesting that an alteration of AR orientation is likely not responsible for the marked differences in precipitation changes. Dynamical changes in IVT, assessed using the 850-hPa wind speed (e.g., Lavers et al., 2015; Michaelis et al., 2021), are not likely to be responsible considering the negligible differences in relationship between mid-level temperature and mid-level wind speed for both AR pulses across epochs (Figures 5d and 5h). The difference in precipitation enhancements between the two pulses is, therefore, attributable to changes in the relationship between mid-level temperature, moisture, and AR intensity, consistent with the expected thermodynamic response.

During the first pulse, the average mid-level temperature over the FRB increases by $\sim 3^{\circ}\text{C}$ from present to future epochs (Figure 3) while the IVT increases by $\sim 31\%$ (from $\sim 343 \text{ kg m}^{-1} \text{ s}^{-1}$ to $\sim 448 \text{ kg m}^{-1} \text{ s}^{-1}$; Figure 1a). Consistent with the larger precipitation increase, both mid-level temperature and IVT changes are larger during the second pulse with a $\sim 4^{\circ}\text{C}$ increase in temperature (Figure 3) and $\sim 44\%$ increase (from $\sim 346 \text{ kg m}^{-1} \text{ s}^{-1}$ over the FRB to $\sim 498 \text{ kg m}^{-1} \text{ s}^{-1}$) in IVT (Figure 1). Present-to-near-future mid-level temperature and IVT differences follow a similar pattern with a $\sim 1^{\circ}\text{C}$ change in temperature and $\sim 14\%$ increase in IVT during the first pulse followed by a larger $\sim 2^{\circ}\text{C}$ change in temperature and $\sim 21\%$ increase in IVT during the second (Figures 1 and 3). The second AR pulse clearly experiences a stronger thermodynamic response to climate change and consequently, a larger increase in precipitation. Further investigation is needed, however, to fully uncover the mechanisms responsible for the different behavior of the two AR pulses under the same climate change conditions. One hypothesis is that orientation relative to coastal and local topography may modulate the AR-generated precipitation response to global warming. Under present-day conditions, Hecht and Cordeira (2017) found that south-southwesterly oriented ARs tend to produce more precipitation. Therefore, it is possible that the southwesterly orientation of the second pulse may have led to a predisposition for precipitation enhancement as a result of

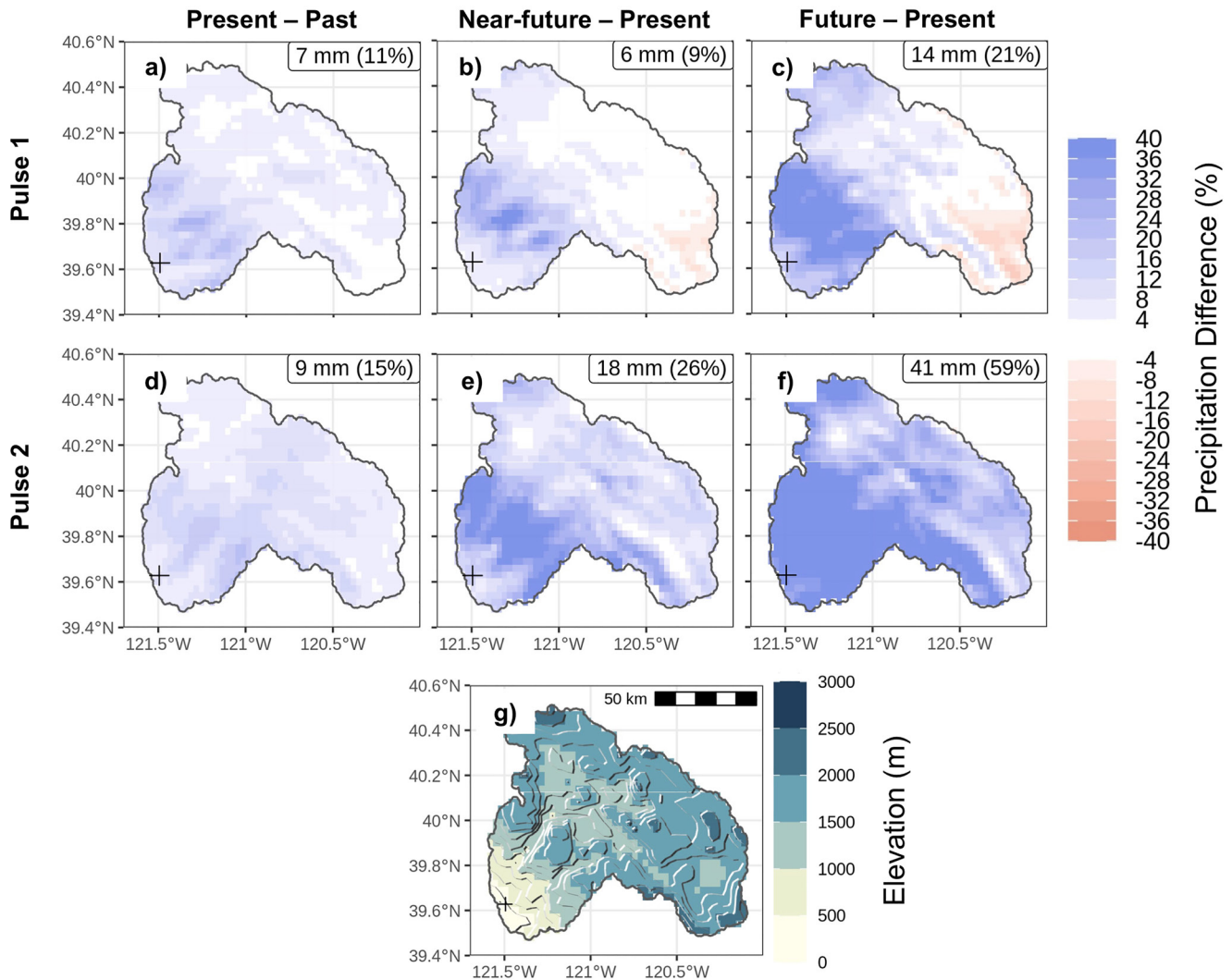


Figure 4. Difference in accumulated precipitation (% change) during the (a–c) first AR pulse from 06 UTC 7 February to 06 UTC 8 February and (d–f) second AR pulse from 03 UTC 9 February to 06 UTC 10 February for MPAS-A ensemble mean (a),(d) present minus past, (b),(e) near-future minus present, and (c),(f) future minus present. (g) Topography throughout the Feather River Basin as represented by MPAS-A. Absolute (mm) and percent changes (%) are reported in the top right corners of (a–f). The Oroville Dam location is indicated by a “+” in all panels.

increased warming (e.g., through enhanced warm-air advection and moisture flux from the southwest). Examining multiple case studies in the presented framework will help clarify this proposed relationship.

Despite overlapping ensemble spreads, warming clearly influences precipitation over the FRB, particularly during the second AR pulse with a $\sim 17\%$ increase per $^{\circ}\text{C}$ over the four epochs (Figure 5e). The temperature-IVT relationship displays even more clarity and less epochal overlap with a $\sim 13\%$ increase in IVT per $^{\circ}\text{C}$ (Figure 5f). Moreover, breaking this relationship down into its constituent parts, moisture and wind, we see that the thermodynamic enhancement of precipitable water at $\sim 10\%$ per $^{\circ}\text{C}$, just over the 7% suggested by the Clausius-Clapeyron relationship (Allen & Ingram, 2002; Held & Soden, 2006) is overwhelmingly responsible for the temperature-IVT relation (Figure 5g). A dynamical contribution via changes in wind speed appears small with a marginal $\sim 4\%$ increase per $^{\circ}\text{C}$ (Figure 5h). Consistent with previous work, the thermodynamic enhancement of moisture in the Oroville AR is overwhelmingly responsible for the global warming induced precipitation increase over the FRB; the warmer, and consequently moister, simulated Oroville AR of near-future and future epochs produces more orographic precipitation (e.g., Baek & Lora, 2021; Gershunov et al., 2019; Ma et al., 2020; Mahoney et al., 2018).

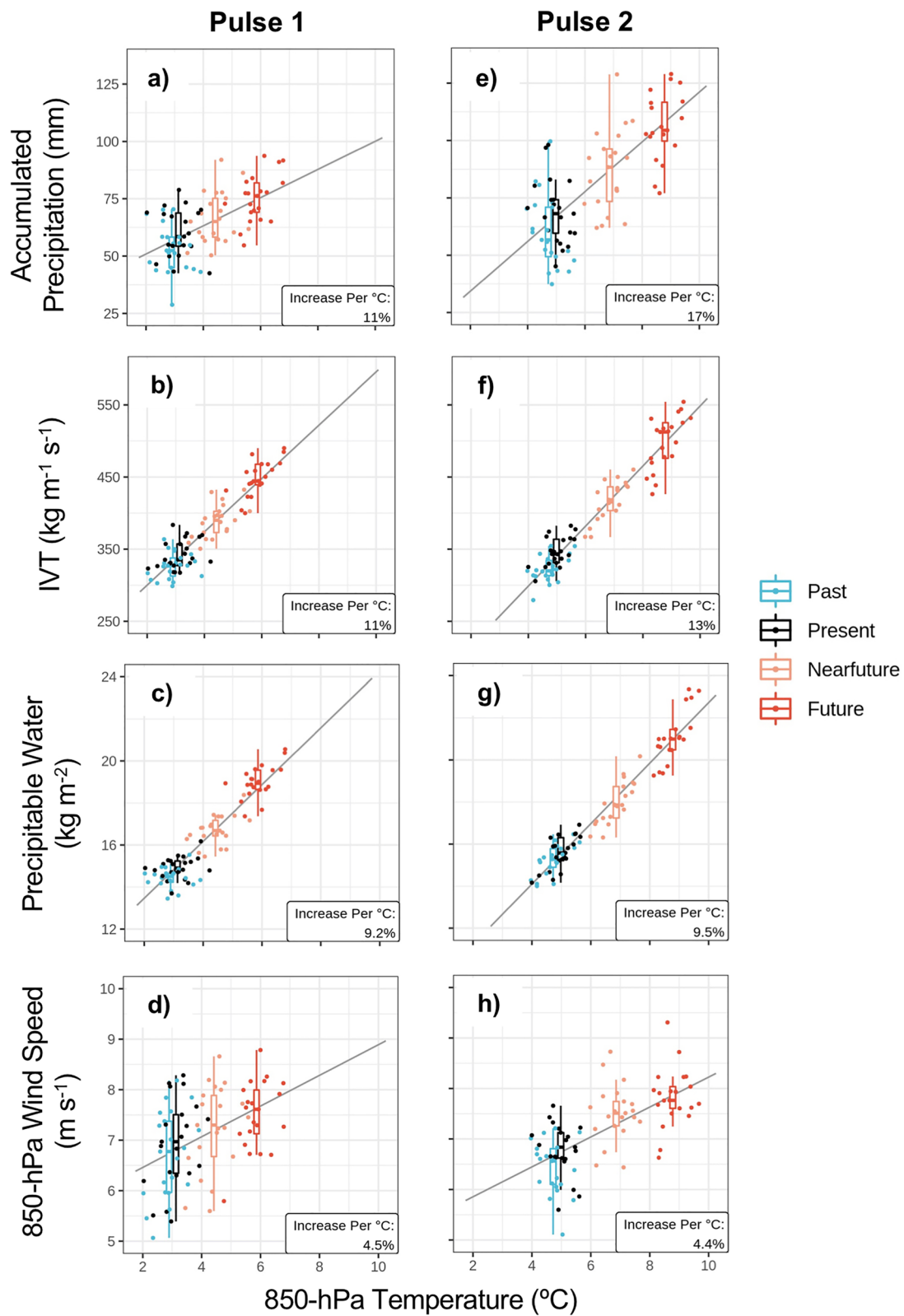


Figure 5.

5. Discussion and Conclusions

Assessing impacts of climate change on precipitation from ARs is rather straightforward, arguably more so than for other storm types since precipitation produced by ARs is mostly orographic in nature (Neiman et al., 2008; Ralph et al., 2005). Assuming no significant changes in dynamics, and given the stationarity of the mountain ranges on the timescales involved, changes in atmospheric moisture ($\sim 7\%$ per $^{\circ}\text{C}$ as estimated by the Clausius-Clapeyron relationship) appear to translate simply to IVT and to precipitation. As such, estimated enhancements to the accumulated precipitation during the Oroville AR over the FRB are commensurate with accelerating projected warming. Importantly, as the magnitude of change increases with warming, the spatial pattern of precipitation enhancement remains stable through time. The orographic nature of this pattern is governed mainly by the enhancement of the AR potency (i.e., moisture) via the temperature dependence of the saturation vapor pressure (i.e., the Clausius-Clapeyron relation).

When we look closer at the two pulses comprising the Oroville AR, however, matters become more complicated. As in many human families, the two Oroville AR siblings display different personalities as they respond to outside stimuli (i.e., to the changing world around them). During the first, westerly-oriented, cooler pulse, precipitation over the FRB increased less from present-day to the late-21st century and exhibits weaker relationships between mid-level temperature, precipitation, and IVT. On the other hand, during the second, southwesterly-oriented, warmer pulse, precipitation drastically increases with warming and a stronger thermodynamic relationship between mid-level temperature, precipitation, and AR intensity is apparent. Dynamical changes during both pulses remain nominal. We hypothesize that AR precipitation efficiency and sensitivity to climate change may be related to, and may depend on, the orientation of vapor transport relative to the local topography. A detailed investigation of such complexity is outside the scope of the current work but will be the subject of a future inquiry.

Such AR family dynamics provide a partial answer to why—although climate change, as we show here, has already contributed notably to precipitation from the Oroville AR—we have not yet clearly observed a trend in AR-related precipitation over our 70+ years of record (Baek & Lora, 2021; Gershunov et al., 2019). Moreover, the volatility of California's hydroclimate is impressive, which is certainly related to the outsized role of extreme precipitation events (Dettinger et al., 2011) and the complexity of AR personalities. Natural variability of the region's volatile hydroclimate is projected to strengthen (Gershunov et al., 2019; Polade et al., 2014, 2017; Swain et al., 2018) and this process has likely already started in the early 21st century with ARs playing a major role (Gershunov et al., 2019).

With continued global warming, we expect to soon see the anthropogenic trend emerge from natural variability in AR-related precipitation in California and other AR-targeted regions, as we have already seen it emerge in the more directly impacted features of the regional climate (e.g., extreme temperature and heat waves (AghaKouchak et al., 2020; Gershunov et al., 2009; Gershunov & Guirguis, 2012; Hao et al., 2018; Li et al., 2020; Wang et al., 2020)). Warming is already exacerbating drought in the West (Cayan et al., 2010; Williams et al., 2020), making retention of water in reservoirs that much more critical. The recent unprecedented heat wave and drought over the southwestern U.S., including California, in June 2021 is a prime example. As a result, record low water levels at Oroville Dam caused the first ever shut down of the hydroelectric power plant going into late summer—the hottest time of year for the region.

The Oroville Dam crisis of February 2017 cost $\sim \$1$ billion in dam repairs (Henn et al., 2020); additional, unknown individual, private costs included relocation expenses incurred due to the evacuation of 188,000 downstream residents (Henn et al., 2020; Vano et al., 2018; White et al., 2019). The complexity of this issue suggests that additional work is needed to sufficiently assess the impacts of climate change on existing engineered infrastructure and design of future dams. Furthermore, future economic damages from enhanced ARs and other weather extremes, can, and should, be estimated (Corringham et al., 2019; Prince et al., 2021; Rhoades et al., 2020). The nonstationary nature of our climate system, particularly that due to human activity, manifesting on timescales of

Figure 5. MPAS-A 850-hPa temperature ($^{\circ}\text{C}$) versus (a),(e) accumulated precipitation (mm), (b),(f) IVT ($\text{kg m}^{-1} \text{s}^{-1}$), (c),(g) precipitable water (kg m^{-2}), and (d),(h) 850-hPa wind speed (m s^{-1}) over the (a)–(d) first AR pulse from 06 UTC 7 February to 06 UTC 8 February and (e)–(h) second AR pulse from 03 UTC 9 February to 06 UTC 10 February for the (blue) past, (black) present, (orange) near-future, and (red) future epochs. All values have been time-averaged over the pulse duration and spatially averaged over the Feather River Basin. In all panels and for all epochs, the ensemble mean and spread are denoted by the box-and-whisker plots and the individual ensemble members are shown by filled circles. Percent increases per $^{\circ}\text{C}$ for all quantities are reported in the bottom right corners of each panel as calculated from the linear regression shown in the solid gray lines.

several human generations, requires a continual recalculation and readjustment of risks due to the changing nature of specific weather extremes as the climate crisis and global society's responses to it evolve.

In future work, our results for past, present-day, and projected future climates will be extended to other notable case studies and funneled through hydrologic models to quantify impacts on runoff and reservoir inflow. This problem is complicated, however, by the necessity to examine changes in preexisting surface conditions such as soil moisture (Cao et al., 2020) and snowpack (Li et al., 2019) leading up to the storm in question. Runoff and reservoir inflow modeling should also assess elevated snowlines associated with the AR itself, which certainly impacted runoff efficiency beyond the overall precipitation increases considered here. For example, it is important to determine how the runoff into the dam from a predominately rain event in the future compares to reservoir inflow from the same mixed-phase event with rain-on-snow induced snow melt in the present-day. Another limitation is that we considered only the aggressive RCP8.5 (“business as usual”) emissions scenario. Projections for the near-future epoch (~2050), however, are robust to emissions scenarios (Franco et al., 2018) and should reflect the near future we are facing irrespective of global mitigation efforts. Our results for the future end-of-the-century epoch are certainly sensitive to future emissions and represent the worst-case scenario. Impacts of mitigation strategies should, and will, be examined in future work based on the new CMIP6-generation models and scenarios coming online now.

Data Availability Statement

Model output from the simulations presented in this manuscript is located on the local computing cluster at the Center for Western Weather and Water Extremes (CW3E). Please contact the corresponding author for details on accessing these data.

Acknowledgments

Our research was supported by the, California Department of Water Resources (DWR) AR Program, and U.S. Bureau of Reclamation project R15AC00003. This study also contributes to the Department of Interior (DOI) Southwest Climate Adaptation Science Center activities and the National Oceanic and Atmospheric Administration (NOAA) California and Nevada Applications Program award NA11OAR43101. Alexander Weyant was partially supported by the undergraduate Summer URS David Marc Belkin Memorial Research Scholarship for Environment and Ecology. Meredith A. Fish was supported by the Rhodium Group as part of the Climate Impact Lab consortium. The MPAS-A and NCAR Command Language (NCL) are made available by the National Center for Atmospheric Research (NCAR), sponsored by the National Science Foundation (NSF). High-performance computing support from Cheyenne (<https://doi.org/10.5065/D6RX99HX>) was provided by NCAR's Computational and Information System Laboratory, also sponsored by the NSF.

References

- AghaKouchak, A., Chiang, F., Huning, L. S., Love, C. A., Mallakpour, I., Mazdiyasi, O., et al. (2020). Climate extremes and compound hazards in a warming world. *Annual Review of Earth and Planetary Sciences*, 48, 519–548. <https://doi.org/10.1146/annurev-earth-071719-055228>
- Allen, M. R., & Ingram, W. J. (2002). Constraints on future changes in climate and the hydrological cycle. *Nature*, 419, 228–232. <https://doi.org/10.1038/nature01092>
- Baek, S. H., & Lora, J. M. (2021). Counterbalancing influences of aerosols and greenhouse gases on atmospheric rivers. *Nature Climate Change*. <https://doi.org/10.1038/s41558-021-01166-8>
- Cao, Q., Gershunov, A., Shulgina, T., Ralph, F. M., Sun, N., & Lettenmaier, D. P. (2020). Floods due to atmospheric rivers along the U.S. West Coast: The role of antecedent soil moisture in a warming climate. *Journal of Hydrometeorology*, 21, 1827–1845. <https://doi.org/10.1175/JHM-D-19-0242.1>
- Cayan, D. R., Das, T., Pierce, D. W., Barnett, T. P., Tyree, M., & Gershunov, A. (2010). Future dryness in the southwest US and the hydrology of the early 21st century drought. *Proceedings of the National Academy of Sciences USA*, 107(50), 21271–21276. <https://doi.org/10.1073/pnas.0912391107>
- Cobb, A., Michaelis, A., Iacobellis, S., Ralph, F. M., & Delle Monache, L. (2021). Atmospheric river sectors: Definition and characteristics observed using dropsondes from 2014–20 CalWater and AR recon. *Monthly Weather Review*, 149, 623–644. <https://doi.org/10.1175/MWR-D-20-0177.1>
- Corringham, T. W., Ralph, F. M., Gershunov, A., Cayan, D. R., & Talbot, C. A. (2019). Atmospheric rivers drive flood damages in the western United States. *Science Advances*, 5(12), eaax4631. <https://doi.org/10.1126/sciadv.aax4631>
- Daly, C., Halbleib, M., Smith, J. I., Gibson, W. P., Dogget, M. K., Taylor, G. H., et al. (2008). Physiographically sensitive mapping of climatological temperature and precipitation cross the conterminous, *International Journal of Climatology*, 28, 2031–2064. <https://doi.org/10.1002/joc.1688>
- Dettinger, M. D., Ralph, F. M., Das, T., Neiman, P. J., & Cayan, D. R. (2011). Atmospheric rivers, floods and the water resources of California. *Water*, 3, 445–478. <https://doi.org/10.3390/w3020445>
- Du, Q., Faber, V., & Gunzburger, M. (1999). Centroidal Voroni tessellations: Applications and algorithms. *SIAM Review*, 41(4), 637–676. <https://doi.org/10.1137/s0036144599352836>
- Fish, M. A., Wilson, A. M., & Ralph, F. M. (2019). Atmospheric river families: Definition and associated synoptic conditions. *Journal of Hydro-meteorology*, 20, 2091–2108. <https://doi.org/10.1175/JHM-D-18-0217.1>
- Franco, G. F., Cayan, D. R., Pierce, D. W., Westerling, A. L., & Thorne, J. H. (2018). *Cumulative global CO₂ emissions and their climate impact from local through regional scales*. California's Fourth Climate Change Assessment.
- Gao, Y., Lu, J., Leung, L. R., Yang, Q., Hagos, S., & Qian, Y. (2015). Dynamical and thermodynamical modulations on future changes of land-falling atmospheric rivers over western North America. *Geophysical Research Letters*, 42, 7179–7186. <https://doi.org/10.1002/2015gl065435>
- Gershunov, A., Cayan, D. R., & Iacobellis, S. F. (2009). The great 2006 heat wave over California and Nevada: Signal of an increasing trend. *Journal of Climate*, 22, 6181–6203. <https://doi.org/10.1175/2009JCLI2465.1>
- Gershunov, A., & Guirguis, K. (2012). California heat waves in present and future. *Geophysical Research Letters*, 39, L18710. <https://doi.org/10.1029/2012GL052979>
- Gershunov, A., Shulgina, T., Clemesha, R. E. S., Guirguis, K., Pierce, D. W., Dettinger, M. D., et al. (2019). Precipitation regime change in western North America: The role of atmospheric rivers. *Scientific Reports*, 9, 9944. <https://doi.org/10.1038/s41598-019-46169-w>
- Gershunov, A., Shulgina, T., Ralph, F. M., Lavers, D. A., & Rutz, J. J. (2017). Assessing the climate-scale variability of atmospheric rivers affecting western North America. *Geophysical Research Letters*, 44, 7900–7908. <https://doi.org/10.1002/2017GL074175>

- Guan, B., Molotch, N. P., Waliser, D. E., Fetzer, E. J., & Neiman, P. J. (2010). Extreme snowfall events linked to atmospheric rivers and surface air temperature via satellite measurements. *Geophysical Research Letters*, *37*, L20401. <https://doi.org/10.1029/2010GL044696>
- Hao, Z., Hao, F., Singh, V. P., & Zhang, X. (2018). Changes in the severity of compound drought and hot extremes over global land areas. *Environmental Research Letters*, *13*, 124022. <https://doi.org/10.1088/1748-9326/aaee96>
- Hara, M., Yoshikane, T., Kawase, H., & Kimura, F. (2008). Estimation of the impact of global warming on snow depth in Japan by the pseudo-global-warming method. *Hydrological Research Letters*, *2*, 61–64. <https://doi.org/10.3178/HRL.2.61>
- Hecht, C. W., & Cordeira, J. M. (2017). Characterizing the influence of atmospheric river orientation and intensity on precipitation distributions over North Coastal California. *Geophysical Research Letters*, *44*, 9048–9058. <https://doi.org/10.1002/2017GL074179>
- Held, I. M., & Soden, B. J. (2006). Robust responses of the hydrological cycle to global warming. *Journal of Climate*, *19*(21), 5686–5699. <https://doi.org/10.1175/JCLI3990.1>
- Henn, B., Musselman, K. N., Lestak, L., Ralph, F. M., & Molotch, N. P. (2020). Extreme runoff generation from atmospheric river driven snowmelt during the 2017 Oroville Dam spillways incident. *Geophysical Research Letters*, *47*, e2020GL088189. <https://doi.org/10.1029/2020GL088189>
- Hersbach, H., Bell, B., Berrisford, P., Hirahara, S., Horányi, A., Muñoz-Sabater, J., et al. (2020). The ERA5 global reanalysis. *Quarterly Journal of the Royal Meteorological Society*, *146*, 1999–2049. <https://doi.org/10.1002/qj.3803>
- Huang, X., Swain, D. L., & Hall, A. D. (2020). Future precipitation increase from very high resolution ensemble downscaling of extreme atmospheric river storms in California. *Science Advances*, *6*(29), eaba1323. <https://doi.org/10.1126/sciadv.aba1323>
- Johanson, C. M., & Fu, Q. (2009). Hadley cell widening: Model simulations versus observations. *Journal of Climate*, *22*(10), 2713–2725. <https://doi.org/10.1175/2008JCLI2620.1>
- Knowles, N., Dettinger, M. D., & Cayan, D. R. (2006). Trends in snowfall versus rainfall in the western United States. *Journal of Climate*, *19*(18), 4545–4559. <https://doi.org/10.1175/JCLI3850.1>
- Kossin, J. P., Hall, T., Knutson, T., Kunkel, K. E., Trapp, R. J., Waliser, D. E., et al. (2017). *Climate Science Special Report: Fourth National Climate Assessment* (Vol. I). <https://doi.org/10.7930/J07S7KXX>
- Lackmann, G. (2013). The south-central U.S. Flood of May 2010: Present and Future. *Journal of Climate*, *26*(13), 4688–4709. <https://doi.org/10.1175/JCLI-D-12-00392.1>
- Lavers, D. A., Ralph, F. M., Waliser, D. E., Gershunov, A., & Dettinger, M. D. (2015). Climate change intensification of horizontal water vapor transport in CMIP5. *Geophysical Research Letters*, *42*, 5617–5625. <https://doi.org/10.1002/2015GL064672>
- Li, D., Lettenmaier, D. P., Margulis, S. A., & Andreadis, K. (2019). The role of rain-on-snow in flooding over the conterminous United States. *Water Resources Research*, *55*, 8492–8513. <https://doi.org/10.1029/2019WR024950>
- Li, D., Yuan, J., & Kopp, R. E. (2020). Escalating global exposure to compound heat-humidity extremes with warming. *Environmental Research Letters*, *15*(6), 064003. <https://doi.org/10.1088/1748-9326/ab7d04>
- Luković, J., Chiang, J. C., Blagojević, D., & Sekulić, A. (2021). A later onset of the rainy season in California. *Geophysical Research Letters*, *48*, e2020GL090350. <https://doi.org/10.1029/2020GL090350>
- Ma, W., Norris, J., & Chen, G. (2020). Projected changes to extreme precipitation along North American West Coast from the CESM large ensemble. *Geophysical Research Letters*, *47*(1), e2019GL096038. <https://doi.org/10.1029/2019GL086038>
- Mahoney, K., Swales, D., Mueller, M. J., Alexander, M., Hughes, M., & Malloy, K. (2018). An examination of an inland-penetrating atmospheric river flood event under potential future thermodynamic conditions. *Journal of Climate*, *31*(16), 6281–6297. <https://doi.org/10.1175/JCLI-D-18-0118.1>
- Mallard, M. S., Lackmann, G. M., Ayyer, A., & Hill, K. (2013). Atlantic hurricanes and climate change. Part I: Experimental design and isolation of thermodynamic effects. *Journal of Climate*, *26*(13), 4876–4893. <https://doi.org/10.1175/JCLI-D-12-00182.1>
- Margulis, S. A., Cortés, G., Giroto, M., & Durand, M. (2016). A landsat-era Sierra Nevada snow reanalysis (1985–2015). *Journal of Hydrometeorology*, *17*(4), 1203–1221. <https://doi.org/10.1175/JHM-D-15-0177.1>
- Meinshausen, M., Smith, S. J., Calvin, K., Daniel, J. S., Kainuma, M. L. T., Lamarque, J.-F., et al. (2011). The RCP greenhouse gas concentrations and their extensions from 1765 to 2300. *Climatic Change*, *109*, 213–241. <https://doi.org/10.1007/s10584-011-0156-z>
- Michaelis, A. C., Lackmann, G. M., & Robinson, W. A. (2019). Evaluation of a unique approach to high resolution climate modeling using the Model for Prediction across Scales – Atmosphere (MPAS-A) version 5.1. *Geoscientific Model Development*, *12*, 3725–3743. <https://doi.org/10.5194/gmd-12-3725-2019>
- Michaelis, A. C., Martin, A. C., Fish, M. A., Hecht, C. W., & Ralph, F. M. (2021). Modulation of atmospheric rivers by mesoscale frontal waves and latent heating: Comparison of two U.S. West Coast events. *Monthly Weather Review*, *149*(8), 2755–2766. <https://doi.org/10.1175/MWR-D-20-0364.1>
- Moore, B. J., White, A. B., Gottas, D. J., & Neiman, P. J. (2020). Extreme precipitation events in Northern California during winter 2016–17: Multiscale analysis and climatological perspective. *Monthly Weather Review*, *148*(3), 1049–1074. <https://doi.org/10.1175/MWR-D-19-0242.1>
- Mote, P. W., Li, S., Lettenmaier, D. P., Xiao, M., & Engel, R. (2019). Dramatic declines in snowpack in the western US. *Climate and Atmospheric Science*, *2*, 1–6. <https://doi.org/10.1038/s41612-018-0012-1>
- Neiman, P. J., Ralph, F. M., Moore, B. J., Hughes, M., Mahoney, K. M., Cordeira, J. M., & Dettinger, M. D. (2013). The landfall and inland penetration of a flood-producing Atmospheric river in Arizona. Part I: Observed synoptic-scale, orographic, and hydrometeorological characteristics. *Journal of Hydrometeorology*, *14*(2), 460–484. <https://doi.org/10.1175/JHM-D-12-0101.1>
- Neiman, P. J., Ralph, F. M., Wick, G. A., Lundquist, J. D., & Dettinger, M. D. (2008). Meteorological characteristics and overland precipitation impacts of atmospheric rivers affecting the West Coast of North America based on eight years of SSM/I satellite observations. *Journal of Hydrometeorology*, *9*(1), 22–47. <https://doi.org/10.1175/2007JHM855.1>
- Park, S.-H., Klemp, J. B., & Skamarock, W. C. (2014). A comparison of mesh refinement in the global MPAS-A and WRF models using an idealized normal-mode baroclinic wave simulation. *Monthly Weather Review*, *142*(10), 3614–3634. <https://doi.org/10.1175/MWR-D-14-00004.1>
- Payne, A. E., Demory, M. E., Leung, L. R., Ramos, A. M., Shields, C. A., Rutz, J. J., et al. (2020). Responses and impacts of atmospheric rivers to climate change. *Nature Reviews Earth & Environment*, *1*, 143–157. <https://doi.org/10.1038/s43017-020-0030-5>
- Pierce, D. W., Cayan, D. R., Das, T., Maurer, E. P., Miller, N. L., Bao, Y., et al. (2013). The key role of heavy precipitation events in climate model disagreements of future annual precipitation changes in California. *Journal of Climate*, *26*(16), 5879–5896. <https://doi.org/10.1175/JCLI-D-12-00766.1>
- Polade, S. D., Gershunov, A., Cayan, D. R., Dettinger, M. D., & Pierce, D. W. (2017). Precipitation in a warming world: Assessing projected hydro-climate changes in California and other Mediterranean climate regions. *Scientific Reports*, *7*, 10783. <https://doi.org/10.1038/s41598-017-11285-y>
- Polade, S. D., Pierce, D. W., Cayan, D. R., Gershunov, A., & Dettinger, M. D. (2014). The key role of dry days in changing regional climate and precipitation regimes. *Scientific Reports*, *4*, 4364. <https://doi.org/10.1038/srep04364>

- Prince, H. D., Gibson, P. B., DeFlorio, M. J., Corringham, T. W., Cobb, A., Guan, B., et al. (2021). Genesis locations of the costliest atmospheric rivers impacting the western United States. *Geophysical Research Letters*, *48*(20), e2021GL093947. <https://doi.org/10.1029/2021GL093947>
- Ralph, F. M., Neiman, P. J., & Rotunno, R. (2005). Drosopside observations in low-level jets over the northeastern Pacific Ocean from CALJET-1998 and PACJET-2001: Mean vertical-profile and atmospheric-river characteristics. *Monthly Weather Review*, *133*(4), 889–910. <https://doi.org/10.1175/MWR2896.1>
- Rasmussen, R., Liu, C., Ikeda, K., Gochis, D., Yates, D., Chen, F., et al. (2011). High-resolution coupled climate runoff simulations of seasonal snowfall over Colorado: A process study of current and warmer climate. *Journal of Climate*, *24*(12), 3015–3048. <https://doi.org/10.1175/2010JCLI3985.1>
- Rhoades, A. M., Jones, A. D., Srivastava, A., Huang, H., O'Brien, T. A., Patricola, C. M., et al. (2020). The shifting scales of western U.S. landfalling atmospheric rivers under climate change. *Geophysical Research Letters*, *47*(17), e2020GL089096. <https://doi.org/10.1029/2020GL089096>
- Rhoades, A. M., Ullrich, P. A., & Zarzycki, C. M. (2018). Projecting 21st century snowpack trends in western USA mountains using variable-resolution CESM. *Climate Dynamics*, *50*, 261–288. <https://doi.org/10.1007/s00382-017-3606-0>
- Schär, C., Frei, C., Lüthi, D., & Davies, H. C. (1996). Surrogate climate-change scenarios for regional climate models. *Geophysical Research Letters*, *23*(6), 669–672. <https://doi.org/10.1029/96GL00265>
- Singh, I., Dominguez, F., Demaria, E., & Walter, J. (2018). Extreme landfalling atmospheric river events in Arizona: Possible future changes. *Journal of Geophysical Research: Atmospheres*, *123*(14), 7076–7097. <https://doi.org/10.1029/2017JD027866>
- Skamarock, W. C., Klemp, J. B., Duda, M. G., Fowler, L. D., Park, S.-H., & Ringler, T. D. (2012). A multiscale nonhydrostatic atmospheric model using centroidal Voroni tessellations and C-grid staggering. *Monthly Weather Review*, *140*(9), 3090–3105. <https://doi.org/10.1175/MWR-D-11-00215.1>
- Swain, D. L., Langenbrunner, B., Neelin, J. D., & Hall, A. (2018). Increasing precipitation volatility in twenty-first century California. *Nature Climate Change*, *8*, 427–433. <https://doi.org/10.1038/s41558-018-0140-y>
- Vano, J. A., Miller, K., Dettinger, M. D., Cifelli, R., Curtis, D., Dufour, A., et al. (2018). Hydroclimate extremes as challenges for the water management community: Lessons from Oroville dam and hurricane Harvey. *Bulletin of the American Meteorological Society*, *100*(1), S9–S14. <https://doi.org/10.1175/BAMS-D-18-0219.1>
- Wang, J., Chen, Y., Tett, S. F. B., Yan, Z., Zhai, P., Feng, J., & Xia, J. (2020). Anthropogenically driven increases in the risks of summertime compound heat extremes. *Nature Communications*, *11*, 528. <https://doi.org/10.1038/s41467-019-14233-8>
- Warner, M. D., Mass, C. F., & Salathé, E. P., Jr. (2015). Changes in winter atmospheric rivers along the North American West Coast in CMIP5 climate models. *Journal of Hydrometeorology*, *16*(1), 118–128. <https://doi.org/10.1175/JHM-D-14-0080.1>
- White, A. B., Moore, B. J., Gottas, D. J., & Neiman, P. J. (2019). Winter storm conditions leading to excessive runoff above California's Oroville Dam during January and February 2017. *Bulletin of the American Meteorological Society*, *100*(1), 55–70. <https://doi.org/10.1175/BAMS-D-18-0091.1>
- Williams, A. P., Cook, E. R., Smerdon, J. E., Cook, B. I., Abatzoglou, J. T., Bolles, K., et al. (2020). Large contribution from anthropogenic warming to an emerging North American megadrought. *Science*, *368*(6488), 314–318. <https://doi.org/10.1126/science.aaz9600>
- Zhang, P., Chen, G., Ma, W., Ming, Y., & Wu, Z. (2021). Robust atmospheric river response to global warming in idealized and comprehensive climate models. *Journal of Climate*, *34*(18), 7717–7734. <https://doi.org/10.1175/JCLI-D-20-1005.1>